AIAA SciTech Forum
January 3-7, 2022, San Diego, CA & Virtual
AIAA SCITECH 2022 Forum

10.2514/6.2022-1733

Green Ionic Liquid Multimode Monopropellant Microthruster

Animesh Sharma[1], Anthony C. Adduci[2], Joshua L. Rovey[3], Zachary R. Putnam[4], Michael F. Lembeck[5]
University of Illinois Urbana-Champaign, Urbana, Illinois, 61801, U.S.A

Charles N. Ryan[6], Chengyu Ma[7]
University of Southampton, Southampton, SO17 1BJ, United Kingdom

Steven P. Berg[8]
Froberg Aerospace, LLC, Wilmington, NC 28401, USA

A chemical microthruster was designed and tested that catalytically decomposes green ionic liquid propellant specifically designed for multimode space propulsion. The monopropellant is called FAM-110A and is synthesized by mixing [Emim][$EtSO_4$] and HAN in the ratio of 59%-41% by weight. The microthruster is designed to produce 0.1 N thrust and fabricated from stainless steel using additive manufacturing. The catalyst is 0.3-mm-diameter Platinum-coated γ alumina. The manufactured thrusters have exit and throat areas that are up to 50% different from the design specifications due to the material type, size, and manufacturing process. The decomposition is achieved by electrically heating the thruster. Several hot fire tests were conducted and for the first time the multimode propellant FAM-110A was demonstrated in traditional catalytic decomposition thrusters. The tests were conducted for catalyst bed temperatures of 120 ºC and 500 ºC, and propellant flow rates of 40 µL/s and 65 µL/s. The highest temperature measured by thermocouples within the thruster interior was 650 ºC.

I. Nomenclature

A	=	Arrhenius pre-exponential factor [mL/mol/s]
A_t	=	Throat Area [m^2]
C_F	=	Thrust coefficient [-]
c^*	=	Characteristic velocity [m/s]
E	=	Activation energy [J]
F	=	Thrust [N]
g_o	=	Gravitational constant [9.81 m/s2]
I_{sp}	=	Specific impulse [s]
T	=	Temperature [K]
k'	=	Reaction rate constant [mL/mol/s]
k_B	=	Boltzmann constant [1.38×10^{-23} J/K]
L	=	Tubing length [m]
$\dot{m}$	=	Mass Flow Rate [kg/s]
P_c	=	Chamber pressure [Pa]

[1] Postdoctoral Researcher, Department of Aerospace Engineering
[2] Graduate Student, Department of Aerospace Engineering
[3] Associate Professor, Department of Aerospace Engineering, AIAA Associate Fellow, rovey@illinois.edu.
[4] Assistant Professor, Department of Aerospace Engineering. AIAA Senior Member
[5] Clinical Associate Professor, Department of Aerospace Engineering.
[6] Lecturer in Astronautics, Engineering and Physical Science, Astronautics Research Group
[7] Postdoctoral Researcher, Engineering and Physical Science, Astronautics Research Group
[8] CEO, AIAA Senior Member

ΔP = Pressure drop [Pa]
Q = Volumetric flow rate [m^3/s]
R = Universal gas constant (8.31446 J/mol-K)
T_c = Chamber temperature [K]
W = Exhaust molecular weight [g/mol]
ρ = Density [kg/m^3]
μ = Dynamic Viscosity [Pa-s]
γ = Ratio of Specific Heats [-]

II. Introduction

Multimode Propulsion (MMP) is a type of spacecraft propulsion that incorporates two or more propulsive modes in a single package with all modes sharing at least some of the same propellant. While multimode systems could be of the same class of propulsion (e.g. a hydrazine monopropellant/bipropellant system), systems utilizing a shared propellant for both high-thrust chemical and high-specific impulse electric thrusters offer the highest degree of maneuver flexibility. MMP may be enabling for a class of missions requiring high thrust for on demand or evasive maneuvers along with efficient low thrust capabilities for less time-critical situations. Furthermore, given the ability to allocate propellant between high and low thrust maneuvers, MMP may be enabling for missions which are not necessarily well defined prior to launch, but which instead can respond to emerging scenarios in situ. The defining characteristic of a MMP system is the use of the same propellant for the two modes, which is necessary to attain full maneuver flexibility. The system, by extension, then would use a single propellant tank (or bank of tanks) that feeds both the chemical and electrospray thrusters. Ideally, some, or all, of the other supporting hardware such as feed lines and electrical components could also be shared between the two modes in order to reduce the system inert mass. This paper will present recent results of a test campaign to study the operational and performance characteristics of a chemical microthruster that uses the electrosprayable monopropellant FAM-110A.

The high thrust of the chemical mode of the multimode system enables maneuvers for rapid orbit insertion and rendezvous applications. The electric mode is suitable for precise station keeping or large, slow orbit change maneuvers [1]–[6]. Use of both propulsive modes allows for a high degree of flexibility for the mission design since all of the aforementioned maneuvers are available on demand. Additionally, sharing of propellant between the modes may result in mass savings due to combining hardware such as tanks, feed lines, and power systems. This reduction in inert mass may result in a more capable system compared to separate individual propulsion systems (hybrid propulsion) even if the individual thruster performance of the MMP system is lower than the hybrid propulsion modes. These mass savings may be particularly enabling for smaller spacecraft where the inert mass fraction is significant compared to the propellant mass fraction [3].

Electrospray has been previously investigated as the electric mode for MMP systems due the suitability of popular propellants, i.e. ionic liquids, to be both high performing electrospray as well as energetic [4], [7], [8]. Recent strides have also been made in low thrust chemical propulsion targeting sub-Newton thrust ranges. These systems use monopropellant thrusters, leveraging their low system complexity and reduced volumes, requiring a single propellant delivery system and a simple thruster comprised of a propellant injector, catalyst bed, and nozzle [8], [9]. This, combined with the fact that electrospray is especially well suited for micropropulsion applications makes a multimode system using an electrospray thruster and chemical microthruster an attractive option.

Various MMP concepts have been studied previously [4]. The MMP system envisioned in this work consists of separate thrusters for chemical mode and electrospray, both sharing a common feed system. The chemical thruster is a monopropellant thruster using Platinum catalyst. The electric mode consists of a porous glass emitter thruster. While initially envisioned as a micropropulsion system, the separate thruster architecture has the advantage of being scalable to larger systems. Chemical monopropellant thrusters of this type have a rich history of use on larger systems and electrospray propulsion could potentially provide high efficiency, high thrust density electric propulsion in the medium term.

A major challenge in developing a MMP system is finding a propellant with the desired properties of being able to undergo chemical decomposition while being electrospray compatible. Desired properties for an ionic liquid used for MMP are high density, low melting temperature, low viscosity, high molecular weight, high surface tension, and high electrical conductivity while having no volatile components that will boil off in vacuum [5]. Donius and Rovey investigated Ionic liquids (IL) as a viable option for MMP propellant [10]. Berg and Rovey investigated imidazole-based ILs paired with HAN and determined a double salt mixture of the two liquids could provide excellent performance in both modes [5]. Fonda-Marsland and Ryan further studied ILs for chemical-electrospray propellants, and described the tradeoff between propellant properties required for each mode [11]. Recently, a mixture of ionic

liquids 1-ethyl-3-methylimidazolium ethyl sulfate ([Emim][$EtSO_4$]) fuel and hydroxylammonium nitrate (HAN) oxidizer has been investigated as a multimode propellant option. This mixture, in a 59:41 oxidizer to fuel ratio by mass, has been found to provide chemical performance and decomposition characteristics similar to other state-of-the-art monopropellants such as hydrazine, LMP-103, and AF-M315E) [5], [12], [13]. These studies have also shown that platinum is an effective catalyst for decomposition of this propellant mixture [14][16][17].

The aforementioned propellant mixture, now known as FAM-110A, has been shown to exhibit stable electrospray in capillary emitters with potentially high performance [13] [18][19]. A previous study used a 100 µm capillary emitter and a pressurized feed system to demonstrate stable electrospray operation down to 0.19 nL/s [19]. Using a Faraday cup and QCM, the specific impulse and thrust were determined to be 412 seconds and 1.09 µN, respectively. Higher performance could be attained if lower flow rates could be achieved, which was a limitation the experimental setup. Recently Lyne et. al demonstrated electrospray of FAM-110A in a multi-capillary emitter thruster [20].

There have been several studies on the decomposition of FAM-110A, but operation of the propellant in a traditional thruster has not yet been explored. In addition to the aforementioned fundamental spot plate testing and other decomposition studies, experiments have been conducted to measure the linear burn rate of the FAM-110A propellant at various pressures. Mundahl et. al measured a linear burn rate of 22.8-26.5 mm/s at 1.5 MPa [11] and Rasmont et. al measured a linear burn rate of 10-15 mm/s at 1 MPa [21]. Broemmelsiek et. al have recently explored the effects of additives on the decomposition of HAN-based liquids like FAM-110A [23].Decomposition of FAM-110A in platinum microtubes has also been studied previously [16][19]. However, in the study presented here, we are implementing a more traditional catalyst monopropellant thruster, specifically in a microthruster (~0.1 N thrust). Microthrusters using an additively manufactured structure operating on catalytic decomposition of high-test peroxide (HTP) have been studied previously [24][12][24]–[27]. The microthruster in the previous studies used 87.5% by wt. aq. solution of hydrogen peroxide and exhibited stable operation and acceptable performance.

This paper describes results from the first ever demonstration of a propellant specifically designed for multimode propulsion in a dedicated catalytic decomposition thruster. The next sections describe the design and experimental results for the FAM-110A monopropellant operating in a chemical microthruster that is designed and fabricated to produce 0.1N thrust at chamber pressure of 8 bars. Section II describes the propellant synthesis process. Section III reviews available propellant decomposition data relevant to this work. Section IV describes the thruster design and manufacturing process. Section V presents the test setup and results of the test campaign. Section VI discusses the results of the data and elucidates the main conclusions of the study including future avenues of research.

III. Propellant

A. Synthesis

The synthesis of the multimode monopropellant FAM-110A was developed in previous studies and is repeated here for reference. Aqueous hydroxyl-ammonium nitrate (HAN) (45-47% HAN in water by weight) was procured from Digital Solid State Propulsion of Reno, NV and neat 1-ethyl-3-methylimidazolium ethyl sulfate, [Emim][$EtSO_4$] (98% purity) was procured from Sigma Aldrich. To obtain crystallized HAN, a measured amount of the aqueous solution is first concentrated up to 90% HAN using a rotary evaporator for ~30 minutes. The remaining water in the solution is then evacuated via an azeotropic vacuum distillation process where the solution is mixed with isopropyl alcohol and left under vacuum (~10^{-6} torr) for over 12 hours. Separately and concurrently, the [Emim][$EtSO_4$] is dried using a rotary evaporator for ~2 hours in order to remove any volatile impurities. Following these processes, the HAN crystals are then dissolved in the [Emim][$EtSO_4$] in the desired 59% HAN to 41% [Emim][$EtSO_4$] ratio, by mass. This mixture is allowed to settle overnight, at which point solid HAN is no longer visible in the mixture. Because this is an energetic liquid mixture, caution should be exercised in all steps of the synthesis process and when handling the prepared mixture. The solution is kept in a sealed container and in a dry box when not in use to help prevent water absorption.

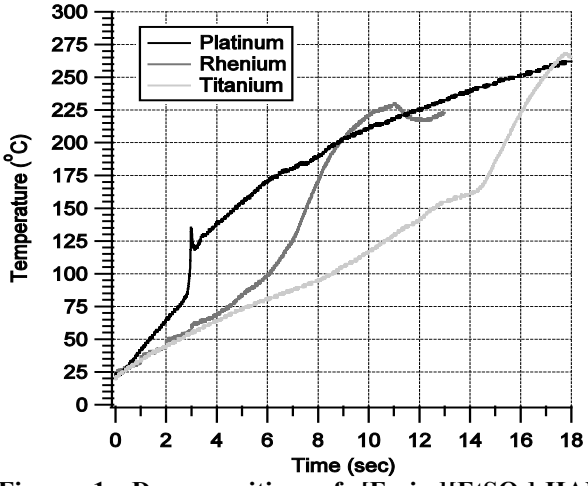

Figure 1. Decomposition of [Emim][$EtSO_4$]-HAN propellant on platinum, rhenium, and titanium surfaces. Reproduced with permission from [13].

B. Decomposition

This section presents results from previous fundamental studies on the decomposition of the FAM-110A monopropellant that are relevant to the present study. These previous studies included catalyst spot plate tests and droplet tests [12], batch reactor tests [15] strand burner tests [28]. The spot plate and droplet tests showed the propellant to be capable of rapid decomposition comparable to state-of-the-art monopropellants including hydrogen peroxide and hydrazine, with the most promising of the catalyst materials tested being iridium and rhenium. The batch reactor tests used a gradually heated thin strip of catalyst foil material to initiate decomposition of the monopropellant, results of which are shown in Figure 1. Temperature just below the propellant droplet was measured throughout the test, allowing for elucidation of a single step Arrhenius reaction rate law, given by Eq. (1),

Table 1. Arrhenius rate equation parameters calculated from batch reactor data. Reproduced with permission from [13].

Material	E/k_B (K)	A (mL/mol-sec)
Platinum	10771 ± 503	(3.87 ± 0.23) x 10^{12}
Rhenium	16170 ± 107	(1.02 ± 0.26) x 10^{17}
Titanium	30111 ± 797	(1.31 ± 0.26) x 10^{19}

$$k' = Ae^{\frac{E}{k_B T}} \tag{1}$$

where the coefficients found from the batch reactor experiment are given in Table 1. It should be noted that platinum was found to be the most active catalyst, having a lower activation energy than rhenium. Finally, a strand burner was utilized to find the linear burn rate of the propellant at various pressures. This test utilized a heated nicrome wire to initiate decomposition of a measured sample of propellant in tube. The wire was made to break and allow the propellant to continue to burn unaided to measure the rate of propagation of the decomposition reaction back into the sample holder. The linear burn rate of the propellant was found to be 10-15 mm/s at 1 MPa [21].

Using the NASA Chemical Equilibrium with Applications (CEA) code, the decomposition products and temperature of the monopropellant decomposition can be predicted. FAM-110A undergoes catalytic decomposition forming predicted products as shown in Eq. 2. The predicted ratio of specific heats and adiabatic flame temperature are calculated to be 1.218 and 1900 K, respectively [15]. These numbers result in a predicted vacuum specific impulse of 254 seconds.

$$C_8H_{16}N_2O_4S + 3.54N_2H_4O_4 \rightarrow 3.54CO_2 + 6.10CO + 8.12H_2O + 6.46H_2 + 4.54N_2 + 0.47H_2S \tag{2}$$

IV. Experimental Setup and Procedure

A. Microthrusters

1. Design and Fabrication

Microthrusters with different dimensions are designed and fabricated for testing with the new propellant FAM-110A. The microthruster design was guided by previous tests of high test peroxide (HTP) microthrusters developed at University of Southampton. [24], [26], [27]. Table 2 shows key dimensions and parameters of the microthrusters selected based on the HTP Microthruster of Southampton. Like the microthrusters tested at Southampton, the microthrusters tested here are designed to generate 0.1 N thrust at atmospheric pressure and chamber pressure of 8 bar. A CAD rendering of a thruster with call-outs to specific parts of the thruster is shown in Figure 1. The thrusters are manufactured using selective laser sintering (SLS) of 316 stainless steel powder. Additive manufacturing makes it easy to include thin-walled instrumentation standpipes at different positions along the length of the thruster. The catalyst used is platinum-based catalyst that has active phase supported on roughly 0.3-mm-diameter γ-alumina

Table 2. Key parameters of the microthrusters tested with high test peroxide at University of Southampton [24],[26],[27].

Parameter	Design Value
Catalyst Bed Dia. [mm]	3.8
Catalyst Bed Length [mm]	7.6
Nozzle Divergence Angle [°]	15
Nozzle Throat Diameter [mm]	0.36
Nozzle Exit Diameter [mm]	0.49

Table 3. Thruster Dimensions

Thruster	Internal Chamber Diameter, mm	Internal Chamber Length, mm	Aspect Ratio, L/D
A1	6.6	19.8	3:1
A2	6.6	19.8	3:1
B1	6.6	13.2	2:1
B2	6.6	13.2	2:1
C1	6.6	6.6	1:1

pellets. The catalyst is held in place by 1.6-mm-thick nickel foam disk. The diffuser and the thruster body are bolted together with a nylon fiber-glass gasket between them. Five thrusters were fabricated with identical dimensions except for the length of decomposition chamber. Three different values of decomposition chamber were selected corresponding to length-to-diameter (L/D) ratios of 1:1, 2:1, and 3:1. The naming convention of each thruster and the internal chamber diameter and decomposition chamber length are given in Table 3.

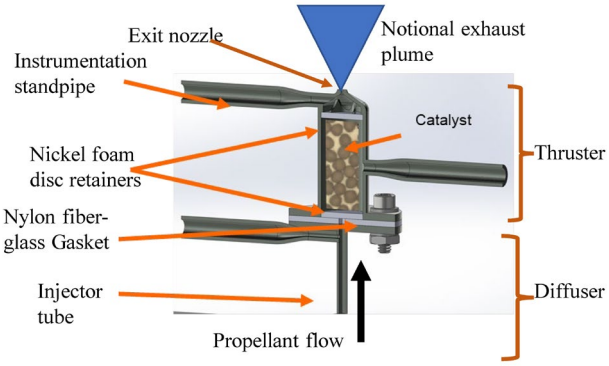

Figure 1. CAD rendering of a microthruster showing the different thruster components and features.

2. Throat and Exit Characterization

The nozzle throat and exit areas were measured for each additively manufactured thruster. Measurements were made using microscope images the looking upstream through the exit orifice of the thrusters. Figure 2 presents the microscope images and the corresponding measured areas for each of the five thrusters. The images show that the exit and throat area surfaces are neither smooth nor circular and are not necessarily concentric. Also shown in this figure is a comparison of the actual measured throat and exit areas for each thruster with the design areas based on the design diameters of the throat and exit, 0.32 and 0.11 mm, respectively. There is significant difference between the design and actual areas, and in some cases the area is smaller (negative difference) than design, while in other cases it is larger (positive percent difference) than design. The throat of the B1 thruster had the largest difference of 51.3% from the design value. The C1 thruster has throat and exit areas that are closest to the design and have percent differences of only 2.2% and 3.4%, respectively. These differences and large variation across thrusters is believed to be due to the type and size of material used in the sintering process, 316 stainless steel powder, and alternative materials such as smaller diameter powder Inconel should be

Figure 3. Water jet from the nozzle of thruster B2.

	0.10mm	A1	A2	B1	B2	C1
Nozzle Exit	Design Area, 0.01mm^2	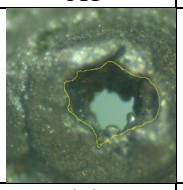	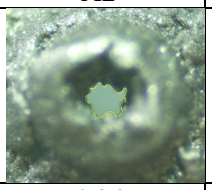	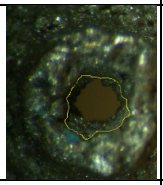	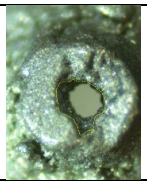	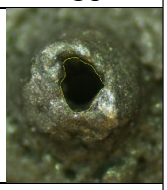
Area, mm^2	Measured	0.3	0.26	0.31	0.21	0.21
	Difference, %	61.2	37.9	78.7	9.8	3.4
Throat	Design Area, 0.08mm^2	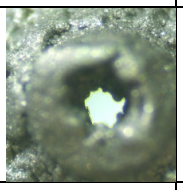	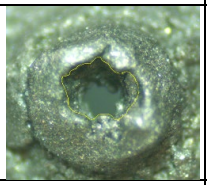	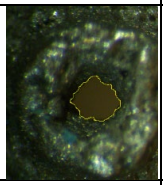	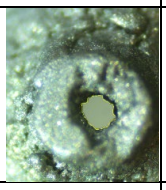	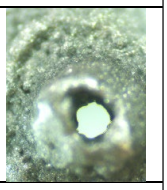
Area, mm^2	Measured	0.07	0.07	0.15	0.09	0.10
	Difference, %	31.2	-32.2	51.3	-9.6	2.2

Figure 2. Optical Images of thruster nozzle exit and throat

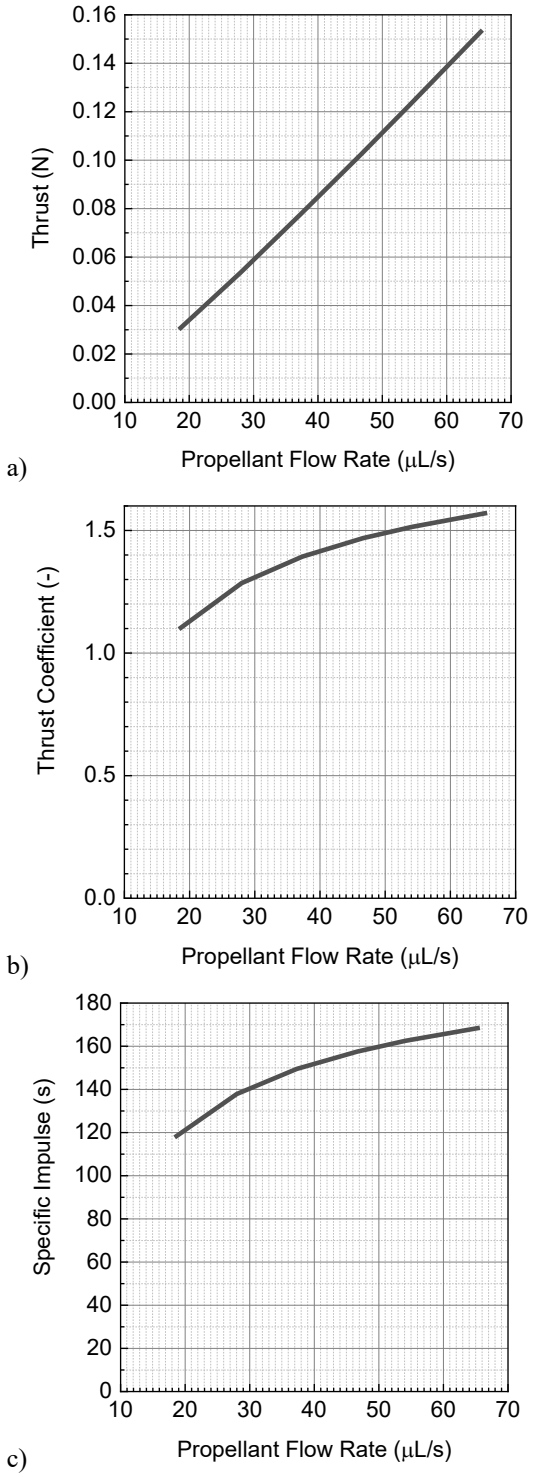

Figure 4. Predicted thruster performance for different propellant flow rates: a) Thrust; b) Thrust Coefficient; and c) Specific Impulse

pursued in the future. These differences and large variations make comparing predicted and actual performance and operation of the thrusters difficult.

A qualitative investigation of the alignment of the thruster nozzle was performed using water. Specifically, water was pressure fed into the thruster and the emerging water jet was visualized. A photograph of this test is shown in Figure 3. The water jet appears to emerge from the thruster in a straight line suggesting the jet (water or gaseous) will produce mostly axial thrust.

B. Predicted Performance

Thruster performance is predicted using a simple model. We assume the mass flow through the thruster is choked at the nozzle throat and the corresponding mass flow is then determined by the chamber pressure, chamber temperature, throat area, and decomposition products molecular weight and specific heat ratio, as shown in Eq. 3. We use the output values from the CEA analysis described previously as inputs to this equation, along with the predicted adiabatic flame temperature. The characteristic velocity, c^*, from CEA simulations was calculated to be 1051.89 m/s. We use the design value of the throat area, instead of the measured values shown in Figure 2, and assume a constant value of 0.101 mm^2.

The mass flow rate in Eq. 3 is gas flow rate (kg/s) of the decomposition products flowing out the nozzle, whereas in an experiment we control the liquid propellant flow rate into the thruster and the corresponding backing or driving pressure required to deliver the desired flow rate. The gaseous mass flow rate is related to the liquid propellant mass flow rate through the mass density of the propellant, $\rho_{FAM110A} = 1.42 \frac{g}{cm^3}$. As the driving pressure increases and the input mass/propellant flow rate increases, the chamber pressure increases. We assume a fixed specific impulse of 180 s and then, as Eq. 4 shows, the thruster is a linear function of the mass flow rate. This relationship is plotted in Figure 4a. The relationship between thrust coefficient and thrust is given by Eq. 5. The thrust coefficient C_F is plotted against propellant flow rate. For 45 $\mu L/s$ the theoretical thrust coefficient is Figure 4b. The specific impulse is calculated for the different propellant flow rate and plotted in Figure 4c.

$$\dot{m} = \frac{A_t P_c \gamma}{\sqrt{\gamma T_c \frac{R}{W}}} \sqrt{\left(\frac{2}{\gamma+1}\right)^{\frac{\gamma+1}{\gamma-1}}} \quad (3)$$

$$F = \dot{m} I_{sp} g_0 \quad (4)$$

$$C_F = F / p_c A_t \quad (5)$$

C. Injector

The microthrusters use a 'Poiseuille' type injector similar to what was used previously in HTP microthrusters. This is basically a small diameter tube directly upstream of the thruster decomposition chamber. This type of injector uses viscous forces to act along the length of the tube to provide high flow impedance and thereby isolate the upstream feed system from any turbulence and pressure fluctuations in the decomposition chamber [29], [30][30], [31]. Here,

we used an injector that is smooth bore 316 stainless steel, 5 cm long, and has internal diameter of 0.508 mm. The pressure drop across the injector is governed by the Hagen-Poiseuille Equation, Eq. 6. The pressure drop due to the injector was calculated by taking the difference of the pressure at upstream and downstream locations of the injector using deionized water. The flow at downstream location was restricted using a needle valve to create a pressure buildup of 126 psig. The flow rate was set at a constant 2 $\mu L/s$ and a pressure drop of 4.64% was measured. However, the measurement yields a value of the liquid viscosity of 660 cP whereas the theoretical value of viscosity for deionized water is about 1 cP.

$$\Delta p = \frac{8\mu L Q}{\pi R^4} \tag{6}$$

D. Catalyst

The thrusters are tested with Pt catalyst 5% by weight supported on γ alumina (gamma alumina) and manufactured by ALB Materials Inc, Nevada (ALB-CAT012). Characterization of the catalyst was done using an optical microscope. Figure 5a). presents the image of unused Pt/Alumina pellets taken at 4.5x zoom using an Amscope Optical Microscope and captured using Microscope Digital Camera 18MP Aptima Color CMOS Camera. It is evident that the pellets are non-uniform in shape and of varying sizes and diameters. The image is used to measure the distributions of the circularity and projected area of the pellets and those results are is shown in Figure 5b. Circularity is a measure of how circular or round the pellets are and a value of 1 would be a perfect circle. There is a distribution in the circularity of the catalyst pellets and the large peak at 0.9 indicates that about 40% of the particles are 90% circular, and about 8% of the pellets are 80% circular. The red curve is the distribution of the project area. The projected area is the two-dimensional view or projected frontal area. For example, the projected area of a sphere is a circle. This can also be thought of as a size distribution of pellets. There is a distribution in the projected area because some pellets are larger or smaller than others. The most probable or peak value of the projected area distribution is at approximately 0.14 mm^2. Assuming a perfectly circular (or spherical) pellet, the most probably diameter is then 0.42 mm. This is larger than the manufacturer stated size of the pellets of 0.4-0.6 mm. The projected area distribution is wide and has a full-width half maximum value of 0.125 mm^2, which is on the order of and almost the same as the most probable projected area. In general, these results suggest that the catalyst pellets are mostly circular (90% circular), but there is a wide variability in their size.

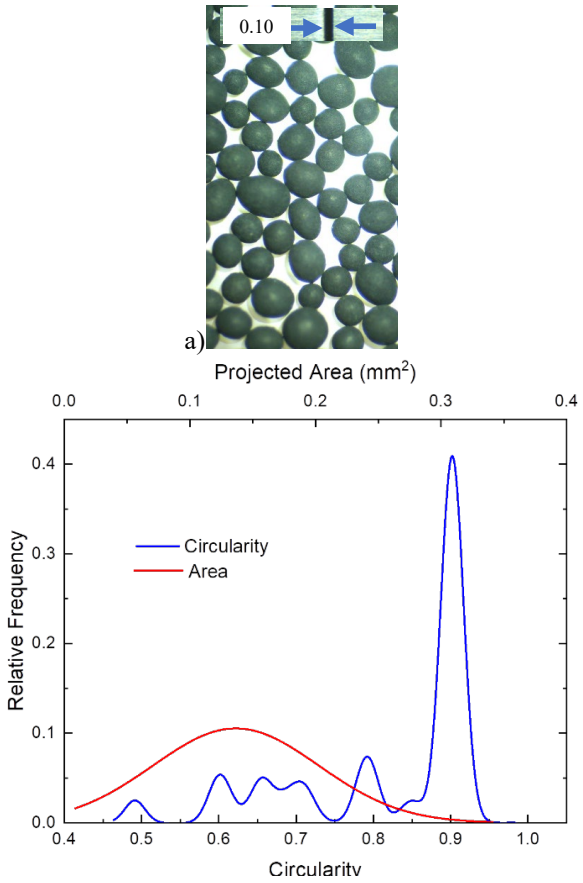

Figure 5. a) Optical image of Pt-coated alumina pellets taken at 4.5x zoom, scale is 0.10 mm b) Circularity and projected area of the Pt-coated alumina pellets

E. Feed System and Preheat Control

A schematic of the feed system is shown in Figure 6. Propellant is fed by a Harvard Apparatus syringe pump at a prescribed flow rate through a series of valves and into the injector and then the thruster. At the injector and thruster, there are four pressure sensors and thermocouples for pressure and temperature measurement, respectively. Specifically, the pressure sensors are Omega PX309-200G5V and are rated to 200 psi with a response time of < 1 ms and an accuracy of 0.5 psi. The thermocouples are K-type 0.5-mm-diameter fast response thermocouples. A pressure sensor is attached at each of the three thruster standoff pipes (as shown in Figure 1) and the fourth is attached to a

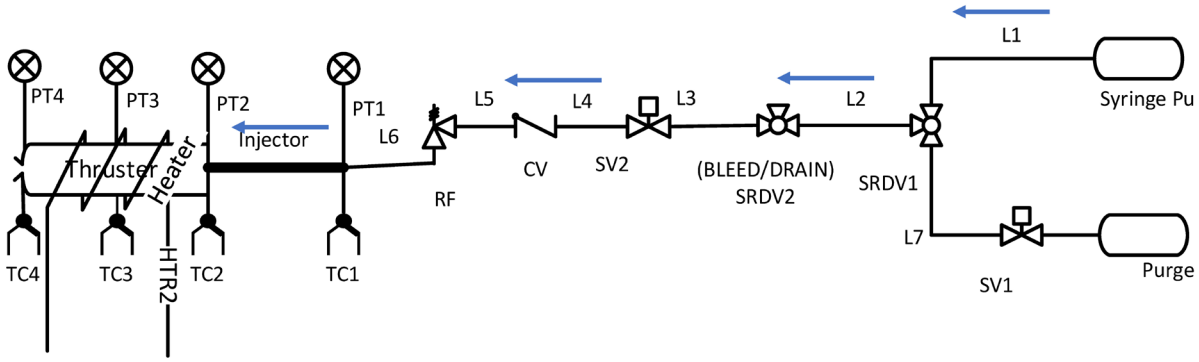

Figure 7. Schematic of the microthruster feed system. Blue arrows show propellant flow direction. PT – pressure transducer, TC – thermocouple.

standoff instrumentation pipe on the upstream side of the injector. The thermocouples are inserted into the thruster through the instrumentation standoff pipes at the same locations. In the following figures and description, we refer to these axial locations of sensor measurements as pre-injector, pre-chamber, mid-chamber, and nozzle plenum locations, which correspond to locations PT/TC1, PT/TC2, PT/TC3, PT/TC4, respectively in Figure 6.

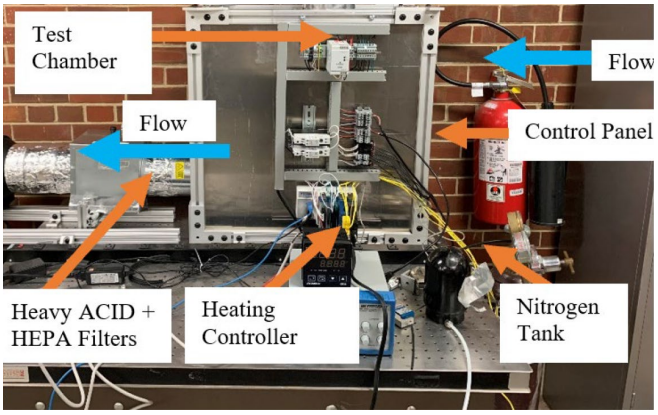

Figure 6. Microthruster Test Facility

Nitrogen purge gas can also be fed through the system. As shown on the right in Figure 6, a gas cylinder of nitrogen can be connected to the system. This is done at the end of a test to purge any remaining propellant from the system. Propellant is forced from the system through the bleed/drain valve, and then any remaining downstream propellant is forced out the thruster exit.

The catalyst bed must be heated in order to initiate and expedite the decomposition of the propellant. The microthruster was wrapped with heater tape and its temperature was controlled with an Omega temperature controller. The feedback temperature used by the controller was the mid-chamber thermocouple temperature.

F. Test Facility

The Micro-thruster Test Facility shown in Figure 7 is in the high-pressure combustion laboratory at Department of Aerospace Engineering at University of Illinois Urbana-Champaign. It is setup and designed for conducting experiments with micro scale chemical thrusters (sub-newton thrust), consuming green ionic liquid monopropellant fuel, at atmospheric pressure. The test chamber is constructed from aluminum panels and has polycarbonate front side for optical axis. The dimension of the chamber is 2'x 2' x1'. Some of the exhaust gases of green ionic liquid monopropellants can be hazardous and therefore the exhaust is quickly removed from the test chamber and exhausted from the building. The exhaust air flow in the test chamber is driven by a 6" dia. 395 cfm ducted fan and filtered by a combination of heavy-duty acid filter and 300 HEPA filter. Downstream of the filter, the exhaust is carried by a 4" diameter flexible aluminum duct. The test chamber sits on a 3' x 4' breadboard and attached to it is a Nitrogen cylinder for purging and temperature controller.

Table 4: Test Facility Instrumentation

Instrument/hardware	Instrument type	Units	Acquisition	Acquisition Rate, Hz
Pressure Transducer	Sputtered thin film	[bar]	NI-9205	1000
Thermocouple	K Type	[°C]	NI-9212	5
Load cell	Single Point Balanced	[N]	NI-9237	800

The Control Panel houses the 120VAC and 24V DC power distribution to the valves and sensors, and NI DAQ based instrumentation and control systems. At present there are four K-type 0.5mm diameter fast response thermocouples for temperature measurements, four pressure transducers for pressure measurements up to 200 psig, and 20 lbf load cells installed. The instrumentation is outlined in Table 4. The facility operation is managed remotely from a control room through LabVIEW based Control Center.

G. Procedure

Pressure and temperature measurements were acquired during hot fire tests of microthrusters. Before doing hot fire tests, the system was operated on water to verify the remote control of the apparatus and the procedures. The microthruster was attached to the feed system and all system were verified to be working properly before loading any propellant. Approximately 30 mL of the FAM-110A propellant was synthesized and used for a single test. The propellant was loaded into a stainless steel syringe. The syringe was placed into the syringe pump. The exhaust fan was turned on and then personnel evacuated the test facility area such that the system was then operated remotely. The thruster preheat temperature was set by turning on the heating controller. When the thruster reached its desired preheat temperature, the valves between the syringe pump and thruster were opened and the syringe pump was commanded to begin flowing propellant. The data acquisition system recorded pressure and temperature throughout the entire process. When the syringe was empty, the thruster ceases to operate and the temperature and pressure decrease and the test was complete. When the thruster was cooled back to room temperature, the drain valve was opened and nitrogen purge gas used to flush the system of propellant remaining in the feed lines.

V. Results

Hot fire tests were conducted with A1 and C1 thrusters for 40 µL/s and 65 µL/s propellant flow rate and thruster preheat temperature of 120 ºC and 500 ºC. Figure 8 presents the pressure and temperature measurements at pre-injector, pre-chamber, mid-chamber, and nozzle plenum location for the A1 thruster with aspect ratio of 3:1 at 500 ºC pre-heat temperature and 65 µL/s flow rate. The propellant reaches the thruster at 100 s and undergoes decomposition upon meeting the heated catalyst. At times before 100 s, the temperature at the pre-injector is room temperature, while the other three thermocouples in the thruster show elevated temperature due to the electrical pre-heating of the thruster. In particular, the mid-chamber location is the location used as feedback to the temperature controller and therefore is at the set point temperature of 500 C.

The syringe reservoir from which propellant is fed is empty at 200 s. At this time, after 100 s of runtime, the temperature at the exit plenum is still increasing and at 200 s reaches a temperature of 650.6 C. While the syringe pump has stopped, pressure in the feed system lines continues to cause propellant to flow into the thruster. At approximately 280 s the pressure peaks at the pre-injector location and begins to decrease. The valve directly downstream of the syringe pump is closed at 350 s and there is a high-pressure spike in the pressure traces.

The pressure spikes during the hot fire tests are indicative of FAM decomposition. These spikes however are not present at pre injector location indicating that injector has isolated the the pressure fluctuation inside the chamber from reaching

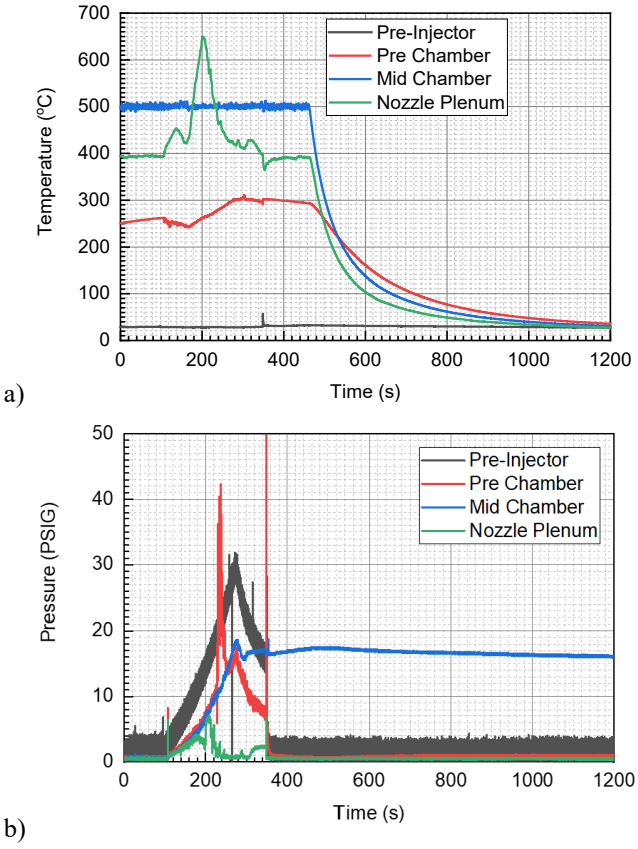

Figure 8. Hot fire test results for the A1 thruster with 3:1 aspect ratio with 500 ºC catalyst pre-heat temperature and 65 µL/s flow rate. a) Temperature b) pressure as a function of time at the four locations.

upstream. The temperature reached a maximum of 650.59 ºC at the nozzle plenum. The mid chamber temperature is steady at 500ºC which is the control temperature. Thus, the propellant decomposition achieved higher temperature at the end of the chamber. The results for the other hot fire tests are summarized in Table 5.

Table 5. Maximum Chamber Temperature and chamber Pressure achieved in Hot Fire Tests

Test Name	Thruster-Aspect Ratio	Flow Rate, $\mu L/s$	Catalyst Preheat Temperature, ºC	Max. Chamber Temperature, ºC	Max Chamber Pressure Measured, PSIG
HFT1	A1 - 3:1	40	120	282*	104
HFT2	C1 - 1:1	40	120	<120	35.16
HFT3	A1 - 3:1	40	120	182.19	17.36
HFT4	A1 - 3:1	65	500	650.59	39.65

*Surface Temperature

VI. Conclusion

A micro-thruster was designed and fabricated to produce 0.1 N thrust at a chamber pressure of 8 bars operating on the thermal decomposition of FAM-110A. Calculations are presented to evaluate performance of the micro-thruster. The thruster nozzle was analyzed using optical microscope and a variability of up to 51% in the throat area from the design value was observed. This variability will need to be addressed by future improvements in the manufacturing process. Hot fire tests were performed at $40\mu L/s$ and $65\mu L/s$ using a catalyst heating temperature of 120 ºC and 500 ºC. The micro-thruster did run with some startup transients. An operating temperature of 650.6 ºC was observed in the thruster.

Acknowledgments

The authors would like to thank the technicians within the department machine shop for their assistance in manufacturing. The research reported here was partially supported by the Defense Advanced Research Projects Agency Grant No.: HR00112110003. The content of this paper does not necessarily reflect the position or the policy of the Government, and no official endorsement should be inferred

References

[1] C. A. Kluever, "Spacecraft optimization with combined chemical-electric propulsion," *J. Spacecr. Rockets*, vol. 32, no. 2, pp. 378–380, 1995.

[2] C. A. Kluever, "Optimal geostationary orbit transfers using onboard chemical-electric propulsion," *J. Spacecr. Rockets*, vol. 49, no. 6, pp. 1174–1182, 2012.

[3] D. Y. Oh, T. Randolph, S. Kimbrel, and M. Martinez-Sanchez, "End-to-end optimization of chemical-electric orbit-raising missions," *J. Spacecr. Rockets*, vol. 41, no. 5, pp. 831–839, 2004.

[4] J. L. Rovey *et al.*, "Review of multimode space propulsion," in *Progress in Aerospace Sciences*, 2020, vol. 118, p. 100627.

[5] S. P. Berg and J. L. Rovey, "Assessment of imidazole-based ionic liquids as dual-mode spacecraft propellants," *J. Propuls. Power*, vol. 29, no. 2, pp. 339–351, 2013.

[6] G. Falcone et. al, "Mission Performance Assessment of Multimode Propulsion for Satellite Servicing Applications," in *2022 IEEE Aerospace Conference, Big Sky, MT*, 2022.

[7] S. P. Berg and J. L. Rovey, "Assessment of multimode spacecraft micropropulsion systems," *J. Spacecr. Rockets*, vol. 54, no. 3, pp. 592–601, 2017.

[8] D. Krejci and P. Lozano, "Space Propulsion Technology for Small Spacecraft," *Proc. IEEE*, vol. 106, no. 3, pp. 362–378, 2018.

[9] K. Lemmer, "Propulsion for CubeSats," *Acta Astronaut.*, vol. 134, no. January, pp. 231–243, 2017.

[10] B. R. Donius and J. L. Rovey, "Ionic liquid dual-mode spacecraft propulsion assessment," *J. Spacecr. Rockets*, vol. 48, no. 1, pp. 110–123, 2011.

[11] E. Fonda-Marsland and C. Ryan, "Preliminary Ionic Liquid Propellant Selection for Dual-Mode Micro-Propulsion Systems," 2017.

[12] S. Berg and J. Rovey, "Decomposition of Monopropellant Blends of Hydroxylammonium Nitrate and Imidazole-Based Ionic Liquid Fuels," *J. Propuls. Power*, vol. 29, pp. 125–135, 2013.

[13] S. P. Berg and J. L. Rovey, "Decomposition of a double salt ionic liquid monopropellant on heated metallic surfaces," *52nd AIAA/SAE/ASEE Jt. Propuls. Conf. 2016*, pp. 1–8, 2016.

[14] A. J. Mundahl *et al.*, "Characterization of a novel ionic liquid monopropellant for multi-mode propulsion," in *53rd AIAA/SAE/ASEE Joint Propulsion Conference*, 2017, p. 4756.
[15] S. P. Berg and J. L. Rovey, "Decomposition of double salt ionic liquid monopropellant in a microtube for multi-mode micropropulsion applications," *53rd AIAA/SAE/ASEE Jt. Propuls. Conf. 2017*, no. July, pp. 1–14, 2017.
[16] M. J. Wainwright, J. L. Rovey, S. W. Miller, B. D. Prince, and S. P. Berg, "Hydroxylammonium nitrate species in a monopropellant electrospray plume," *J. Propuls. Power*, vol. 35, no. 5, pp. 922–929, 2019.
[17] M. J. Wainwright, J. L. Rovey, S. W. Miller, and B. D. Prince, "Experimental investigation of mixtures of 1-ethyl-3-methylimidazolium ethyl sulfate and ethylammonium nitrate with electrospray propulsion applications," *AIAA Propuls. Energy Forum Expo. 2019*, no. August, pp. 1–20, 2019.
[18] S. P. Berg, "Development of ionic liquid multi-mode spacecraft micropropulsion systems," p. 164, 2015.
[19] S. P. Berg, J. L. Rovey, B. P. Prince, S. W. Miller, and R. J. Bemish, "Electrospray of and Energetic Ionic Liquid Propellant for Multi-Mode Micropropulsion Applications," in *51st AIAA/ASME/SAE/ASEE Joint Propulsion Conference*, 2015.
[20] C. T. Lyne, J. Rovey, and S. P. Berg, "Monopropellant-Electrospray Multimode Thruster Testing Results: Electrospray Mode," in *AIAA Propulsion and Energy 2021 Forum*, 2021, p. AIAA-2021-3439.
[21] N. Rasmont, E. J. Broemmelsiek, and J. L. Rovey, "Linear burn rate of green ionic liquid multimode monopropellant," *Combust. Flame*, vol. 219, pp. 212–224, 2020.
[22] A. J. Mundahl, S. P. Berg, and J. L. Rovey, "Linear burn rates of monopropellants for multi-mode micropropulsion," *52nd AIAA/SAE/ASEE Jt. Propuls. Conf. 2016*, pp. 1–11, 2016.
[23] E. J. Broemmelsiek, J. L. Rovey, and S. P. Berg, "Effect of Metal Sequestrants on the Decomposition of Hydroxylammonium Nitrate," *Catalysts*, vol. 11, no. 12, p. 1488, 2021.
[24] E. Fonda-marsland, G. Roberts, D. Gibbon, and C. Ryan, "An Investigation into Injector Architecture for Sub-Newton Monopropellant Propulsion," 2019, pp. 1–15.
[25] C. N. Ryan *et al.*, "Experimental validation of a 1-newton hydrogen peroxide thruster," *J. Propuls. Power*, vol. 36, no. 2, pp. 158–166, 2020.
[26] E. Fonda-Marsland, G. Roberts, C. Ryan, and D. Gibbon, "Development of a low-cost 0.1 N high test peroxide thruster using additive manufacturing.," *AIAA Propuls. Energy Forum Expo. 2019*, no. August, pp. 1–17, 2019.
[27] E. Fonda-Marsland, G. T. Roberts, C. N. Ryan, and D. Gibbon, "Methodology for Geometric Optimization and Sizing for Subnewton Monopropellant Catalyst Beds," *J. Propuls. Power*, vol. 37, no. 5, pp. 1–12, 2021.
[28] S. P. Berg, "Development of ionic liquid multi-mode spacecraft micropropulsion systems," 2015.
[29] G. P. Sutton and O. Biblarz, *Rocket propulsion elements*. John Wiley & Sons, 2016.
[30] R. Humble, *Space Propulsion Analysis and Design*. McGraw-Hill Companies,Incorporated, 1995.
[31] D. H. Huang and D. K. Huzel, *Modern Engineering for Design of Liquid-Propellant Rocket Engines*. 1992.